Journal of Institute of Science and Technology, 30(1), 197-209 (2025)
ISSN: 2467-9062 (print), e-ISSN: 2467-9240
https://doi.org/10.3126/jist.v30i1.76562

© IOST, Tribhuvan University
Research Article

IN-SILICO ANALYSIS OF SECONDARY METABOLITES THAT INHIBIT ALDOSE REDUCTASE TARGETING DIABETIC RETINOPATHY

Ranju Khatiwada, Asmita Shrestha, Kabita Gyawali, Siddha Raj Upadhyaya, Rezina Pradhan, Ashish Phuyal, Sishir Bikram KC, Khaga Raj Sharma, Niranjan Parajuli*
Central Department of Chemistry, Institute of Science and Technology, Tribhuvan University, Kirtipur, 44618, Kathmandu, Nepal
** Correspondence: parajuli511@gmail.com*

(Received:** March 12, 2025; **Final Revision:** June 20, 2025; **Accepted:** June 21, 2025**)

ABSTRACT

Diabetic retinopathy (DR) is a harmful microvascular consequence of diabetes. Aldose reductase, an enzyme involved in the polyol pathway during hyperglycaemic conditions, is responsible for DR. Some commercially available enzyme inhibitors, such as epalrestat, zenarestat, etc., are recommended medications to control pathophysiology; nevertheless, most of them have been unable to satisfy the criteria to be considered a good drug choice. This study aims to explore a pool of secondary metabolites associated with their impressive anti-diabetic properties because they are related to undesirable side of the commercial medications currently on the market. We screened the most potent aldose reductase inhibitor via a thorough *in silico* study, which has been reported as good *in vitro* activity against human aldose reductase and rat lens aldose reductase. High-throughput computational techniques were applied to study the potency of 90 metabolites against target proteins. *In silico* pharmacokinetics and toxicity were evaluated for screened metabolites with binding energy less than -9.0 kcal/mol obtained through the molecular docking method. Among selected metabolites, myrciacitrin IV exhibited the best binding affinity (-9.1 kcal/mol and -11.8 kcal/mol) with both proteins and displayed the least band gap energy (3.379 eV), comparable with the standard drug. Further, molecular dynamics (MD) simulation and Molecular Mechanics Generalised-Born Surface Area (MM/GBSA) investigations confirm myrciacitrin IV as a potent drug candidate targeting aldose reductase.

Keywords: Enzyme inhibition, diabetic retinopathy, myrciacitrin IV, natural products

INTRODUCTION

Diabetic retinopathy (DR) is the most prevalent and serious complication of diabetes and the main factor contributing to blindness affecting millions of people worldwide. The length and severity of hyperglycemia are significantly connected to the risk of retinopathy (Klein *et al*., 1989). Following two decades of diabetes mellitus, approximately all people suffering from diabetes around the age of 30 exhibit some signs of retinopathy, and around half develop proliferative retinopathy. The 20-year incidence of any form of retinopathy is around 80% amongst older individuals who need insulin and 20% among those who do not. The prevalence rates of proliferative are 40% and 5% respectively. This microvascular retinal disease is an illness with enhanced capillary permeability, intraretinal hemorrhages, loss of pericytes, microaneurysms, macular edema, and neovascularisation (Hendrick *et al*., 2015). Based on the level of complexity, diabetic retinopathy is classified into three categories: early, intermediate, and advanced (Antonetti *et al*., 2012). Numerous biochemical processes, such as the activation of the polyol pathway and protein kinase C, the enhanced generation of advanced glycation end products, and oxidative stress, have been proposed to explain how hyperglycaemia affects the maturation of microvascular problems (Brownlee, 2005; Geraldes & King, 2010; Giacco & Brownlee, 2010). Aldose reductase (AR), a major target enzyme for treating diabetes problems, is part of the polyol pathway, which has been intensively explored. Aldose reductase is a globular protein with 315 amino acids (Singh Grewal *et al*., 2015). It is essential for the breakdown of hazardous aldehydes formed during lipid peroxidation, such as 4-hydroxy-trans-2-nonenal (HNE) and its glutathione adduct (GS-HNE) (Maccari & Ottanà, 2015). However, in diabetics, glucose moves towards the polyol pathway, where it is responsible for the generation of osmotically active substances such as sorbitol, as well as a drop in NADPH levels, which finally leads to the inhibition of fatty acid synthesis, DNA synthesis, nitric oxide synthesis, oxidative stress, and more (Singh Grewal *et al*., 2015).

The retina, lens, and nerve tissues all contain aldose reductase. When glucose is converted to sorbitol, osmotic stress occurs due to sorbitol accumulation in the retina, lens, nervous tissues, and kidney, which lacks an enzyme that converts sorbitol to fructose, i.e., sorbitol dehydrogenase, resulting in diabetes complications such as retinopathy, for successful remedies, unconventional strategies for reducing oxidative stress and controlling the track of DR are mandatory (Ciulla *et al*., 2003).

The aldose reductase inhibitors (ARIs) diminish the DR by restricting the action caused by AR during hyperglycemic conditions or by controlling the flow of glucose toward the polyol pathway (Grewal *et al*., 2016). ARIs have been tested in animal models and humans to slow down or advert DM-mediated retinal disorders, thus avoiding sorbitol buildup (Banditelli *et al*., 1999). Although numerous manufactured ARIs are in embryonic and clinical trials, epalrestat is the sole FDA-

authorized that is used to treat diabetic nerve damage (Mori *et al*., 2012). Other synthetic ARIs were pulled out due to extremely negative consequences; sorbinil discontinued production due to intolerance (Sarges *et al*., 1988), while tolrestat and zopolrestat produced significant liver malignancies (Sestanj *et al*., 1984; Grewal *et al*., 2020; Nagini *et al*., 2024). Recent research has revealed human and rodent AR-like proteins that share a high average amino acid sequence similarity (67-71%) but differ markedly in their failure to regulate glucose.

The *in silico* approach is a rapidly expanding scientific subject that focuses on the creation of strategies for leveraging software and databases to create and evaluate molecular, biological, and medical data from many sources (Ekins *et al*., 2007). This computer-aided drug design (CADD), a low-cost and time-efficient technology, employs structural perceptions of both structure-based targets and recognized ligands with biological action (ligand-based). Drug companies and research groups from academia are now using a variety of computer-based *in silico* methods to reduce the duration and expense necessary to identify a potent therapy (Macalino *et al*., 2015). Molecular docking prioritizes complex repositories depending on ligands' structure and electronic compatibility to a certain receptor and relies on evidence gained through evaluating an attractive target's 3D structures. This structure-based method analyses the interaction of two molecules' structures and anticipates binding modes and binding affinities of two molecules with known structures (Kolb *et al*., 2009). It predicts the preferred alignment of a ligand to its target when they are coupled together and foretells whether the interactions are activating or inhibiting (Kitchen *et al*., 2004; Ferreira *et al*., 2015).

MATERIALS AND METHODS

Selection of plant-derived aldose reductase inhibitors

This research aims to determine the usual metabolites that most effectively inhibit aldose reductase. From the literature survey, a total of 90 natural metabolites were selected, each having a suitably documented IC_{50} value (wet-lab trial) against rat lens aldose reductase and/or recombinant human aldose reductase.

Preparation of the ligand

The 3D structures of the selected ligands were downloaded from the PubChem, CHEMBL, and Zinc databases in .SDF format. To convert.SDF format to .PDB file format, BIOVIA Discovery software was utilized, and the ligands were optimized using AutoDock Vina and saved in .PDBQT format.

Preparation of Proteins

The crystal structure of rat lens aldose reductase with PDB ID: 3O3R and the human aldose reductase with PDB ID: 4JIR were retrieved from the Protein Data Bank (RCSB, 2025). Protein preparation was carried out globally following established methodology and procedures (Sastry *et al*., 2013). Water molecules and co-crystallized ligands, i.e., $NADP^+$ and epalrestat of human aldose reductase, and NADP of rat lens aldose reductase were eliminated. After preparing clean protein, it was prepared by adding polar hydrogens and saved in .PDBQT format.

Molecular Docking Method

Molecular docking simulations were performed using AutoDock Tools (version 1.5.6) to estimate the binding affinities and characterize the interaction patterns between selected ligands and target proteins. The size of the grid box was 40 × 40 × 40 Å centered at coordinates x = ˍ 5.716, y = 8.026, and z = 17.347. A grid box spacing of 0.375 Å was used to ensure thorough coverage of the active sites of the enzymes. The catalytic residues TYR 48 and HIS 110 were selected as the catalytic diad for both rat lens aldose reductase and human aldose reductase (Sundaram *et al*., 2011; Zhang *et al*., 2013). The docking outcome was viewed with BIOVIA Discovery Studio Visualizer, which displayed the 2-D and 3-D output interaction with the active sites as well as their bond length and graded based on their binding energies using AutoDock Vina algorithms. Stick models depict the H-bonds and interacting residues. The finest output ligand was retained, possessing a low binding affinity, highly efficient hydrogen bonding, and catalytic positions (Agu *et al*., 2023).

In Silico Pharmacokinetics and Toxicity Prediction

This prediction provides insight into the drug's potential effectiveness and suggests whether the evaluated ligands exhibit properties favorable for oral administration. The metabolites' simplified molecular input line system (SMILES) files are presented to the Pro-Tox II and pkCSM web servers. The organ toxicities, LD_{50}, and toxicological endpoints of the ligands were anticipated using Pro-Tox II (Banerjee *et al*., 2018). Further, complete ADMET profiling of the ligand was done by the pkCSM web server (Garg *et al*., 2021).

Density Functional Theory (DFT) Calculations

The reactivity and efficacy of metabolites against aldose reductase were investigated using Gaussian 09 and GaussView 6.0 software. Density functional theory (DFT) analysis was used to determine the lowest unoccupied molecular orbital (LUMO) and highest occupied molecular orbital (HOMO) energy levels. The 3-parameter Becke, Lee-Yang-Parr (B3LYP) correlation function of DFT and the 6-31D (d,p) basis set was used (Dwivedi *et al*., 2015). The B3LYP functional approach offers an excellent combination of computation and accuracy.

The formula for calculating the energy gap was

$$\Delta E_{gap} = E_{LUMO} - E_{HOMO} \quad \text{.....1,}$$

Subsequently, the ionization potential (IP),

$$IP = -E_{HOMO} \quad \text{.....2,}$$

The electron affinity (EA),

$EA = -E_{LUMO}$ ……3,

Global softness (S), $S = 1/\eta$ ……4,

Global Hardness (η), $\eta = \Delta E/2$ …….5,

Electronegativity (χ), $\chi = (I+A)/2 = -\mu$ …….6,

Electrophilicity Index (ω) = $(\mu^2)/2\eta$ ……..7,

Chemical potential (μ) = - χ ……..8,) were estimated using Koopman's approach (Abu-Melha, 2018).

Molecular dynamics simulation

Thermodynamics-based molecular dynamics (MD) simulation is a method that helps study dynamic alterations in protein-ligand complexes (Ganesan *et al.*, 2017). The stability of the predicted protein-ligand complexes was assessed through MD simulations using the GROMACS version 2021.4 (Abraham *et al.*, 2015). The protein topology was prepared using the CHARMM27 force field (Wacha & Lemkul, 2023), and the ligand topology was generated using the SwissParam service (Bugnon *et al.*, 2023). Each protein-ligand complex was solvated using a basic water model within a triclinic simulation box, designed to ensure a minimum distance of 1.0 nm between the complex and the box boundaries. This setup incorporated a stoichiometric intermolecular potential to maintain appropriate spatial separation. The ionization stages of protein residues were assigned based on their expected behavior at physiological pH (7.0), and periodic boundary conditions were applied. Na^+ and Cl^- ions were added using the Monte Carlo ion placement method to achieve electrostatic neutrality.

The molecular dynamics (MD) simulation process consisted of three key stages. First, energy minimization was carried out using the steepest descent algorithm for 5,000 steps to optimize the initial geometry of the system. This was followed by an equilibration phase under constant number of particles, volume, and temperature (NVT ensemble), utilizing the Berendsen thermostat for temperature coupling. In the final equilibration stage, the Parrinello-Rahman barostat was used to maintain constant pressure, ensuring stable NPT conditions throughout the simulation. Ultimately, MD simulations were run for 100 ns under constant pressure (NPT ensemble). Finally, using built-in parameters like gmx_RMSD, gmx_RMSF, gmx_Rg, and gmx_SASA as well as the quality of H-bonds, a comparison study was carried out. OriginPro 2024b was utilized to plot the MD simulation graphs.

Calculations of binding free energy with the Poisson-Boltzmann Surface Area (MM/PBSA) method of molecular mechanics

The binding free energy (ΔG) of protein-ligand complexes was calculated using MM/PBSA following the procedure outlined by (Valdés-Tresanco *et al.*, 2021). By correlating the free energy of the protein and ligand when in the unbound state with that of the bound protein-ligand complex, ΔG was computed.

$$\Delta G_{bind} = \Delta G_{complex} - (\Delta G_{receptor} + \Delta G_{ligand})$$

where, $\Delta G_{complex}$, $\Delta G_{receptor}$, and ΔG_{ligand} represent the total free energies of the complex, receptor, and ligand, respectively.

RESULTS AND DISCUSSION

Molecular Docking Analyses

Ninety secondary metabolites were selected and docked to human aldose reductase (PDB ID 4JIR), with catalytic diads (HIS 110 and TYR 48), considering epalrestat as the standard compound using AutoDock Vina software. Fifty-six metabolites exhibited binding energies equal to or below -8.4 kcal/mol (Table S1). The range of binding energies in metabolites varied from -5.3 kcal/mol to -10.0 kcal/mol. The binding energies and interactions of the top five potent metabolites with the target protein (Table 1) were evaluated. Myrciacitrin IV with a binding energy of -9.1 kcal/mol (Fig. 1d) formed hydrogen bond interactions with both catalytic diads (HIS 110 and TYR 48), and amino acid residue SER 302 also formed Pi-Alkyl bonds and Pi-Pi T-shaped bonds with TRP 79, VAL 47, PRO 218. Similarly, luteolin-7-rutinoside (Fig. 1c) with a binding energy of -9.8 kcal/mol, followed by luteolin 7-o-glucoside (Fig. 1b) showed the strongest binding energy (-9.6 kcal/mol) with a strong interaction with the catalytic site HIS 110 and other amino acid residues. In the same way, engeletin (1.92Å) (Fig. 1a), myrciacitrin IV (2.23Å), and scolymoside (1.96Å) (Fig. 1e) exhibit the shortest H-bond interaction distances. Compared with the standard drug, epalrestat (Fig. 1f), all five listed metabolites have shown potency against the target protein. Various metabolites, including cinnamaldehyde, cuminaldehyde, curcumin, and others, demonstrated strong binding affinity with catalytic diads through hydrogen bond interactions. Similarly, rosmarinic acid displayed hydrogen bond interactions and Pi-Pi stacked interaction, and methyl lucidenate F engaged in hydrogen bonding interactions with HIS 110, TYR 48, LEU 300, and ALA 299 (Table S1), (Fig. S1) & (Fig. S2) (viii) and (ix).

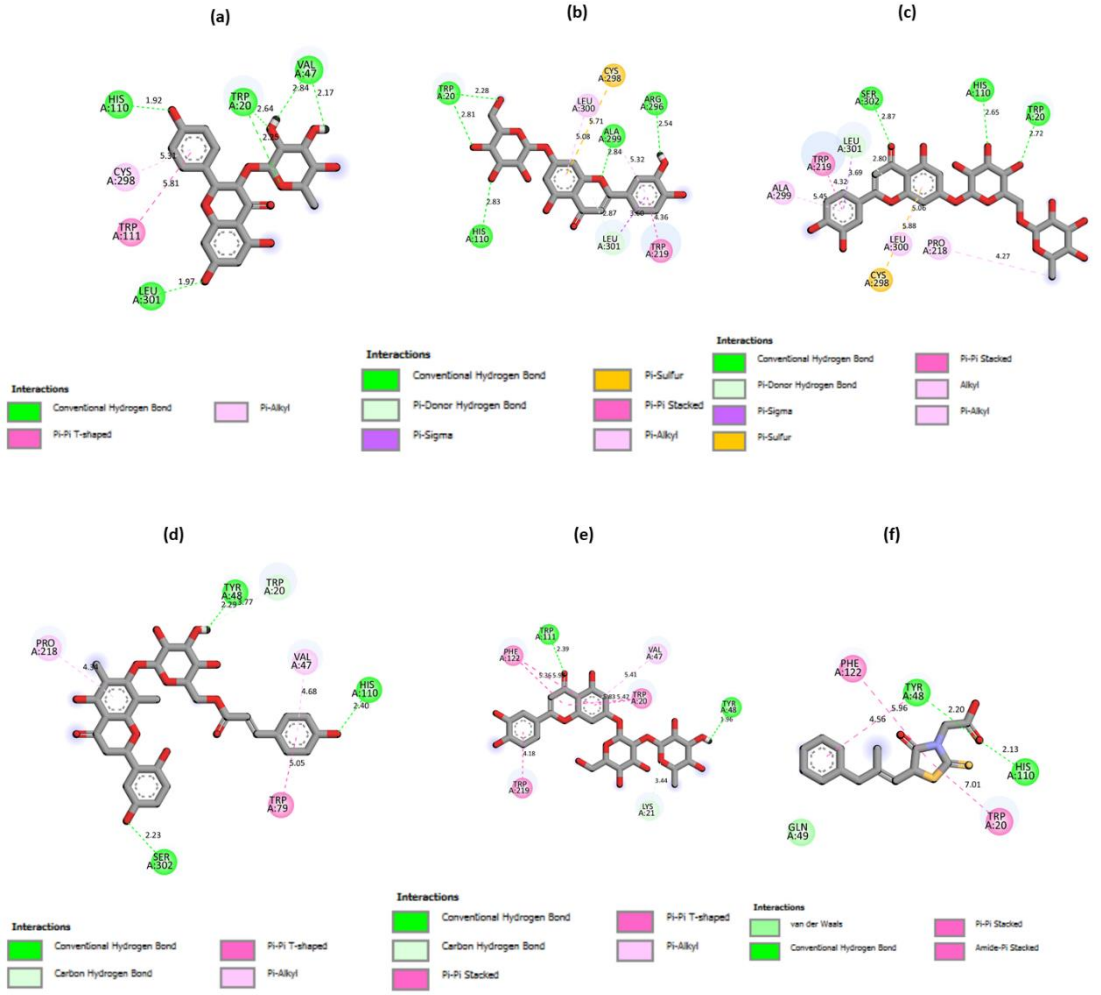

Figure 1. 2D interaction structures of (a) engeletin and (b) luteolin-7-o-glucoside (c) luteolin-7-rutinoside (d) myrciacitrin IV (e) Scolymoside (f) epalrestat complexed with 4JIR.

Table 1. Interaction of Secondary metabolites with human aldose reductase (PDB ID: 4JIR)

Metabolites	Binding Affinity (kcal/mol)	Amino Acid Residues	Interaction Distance Å
epalrestat	-8.4	**TYR 48, HIS 110**, PHE 122, TRP 20, TYR 48	2.20, 2.13, 5.96, 7.01, 4.56
engeletin	-9.0	**HIS 110**, TRP 20, VAL 47, LEU 301, TRP 111, CYS 298,	1.92, 2.64, 2.25, 2.84, 2.17, 1.97, 5.81, 5.31
luteolin-7-O-glucoside	-9.6	**HIS 110**, TRP 20, ALA 299, ARG 296, TRP 219, LEU 300, LEU 301, CYS 298	2.83, 2.28, 2.81, 2.84, 5.32, 2.54, 4.36, 5.08, 3.60, 2.87, 5.71
luteolin-7-rutinoside	-9.8	**HIS 110**, TRP 20, SER 302, TRP 219, ALA 299, LEU 300, PRO 218, LEU 301, CYS 298	2.65, 2.72, 2.87, 4.32, 5.45, 5.06, 4.27, 3.69, 5.88
myrciacitrin IV	-9.1	**HIS 110, TYR 48,** SER 302, TRP 79, PRO 218, VAL 47, TRP 20	2.40, 2.29, 2.23, 5.05, 4.34, 4.68, 3.77
scolymoside	-9.0	**TYR 48**, TRP 111, PHE 122, TRP 20, TRP 219, VAL 47, LYS 21	1.96, 2.39, 5.36, 5.98, 5.83, 5.42, 5.41, 4.18, 3.44

Additionally, all ninety metabolites were docked with rat lens aldose reductase (PDB ID 3O3R), having the catalytic diads (HIS 111 and TYR 49), using epalrestat as the standard drug. Epalrestat (Fig. 2f) showed a binding energy of -8.1 kcal/mol, and seventy-five metabolites exhibited binding energies equal to or below this standard drug. The least binding energies (Table 2) of the top five metabolites, which have also shown remarkable binding affinity and interactions with the target protein, are listed. Myrciacitrin IV displayed strong hydrogen bond interaction with one of the catalytic diads (Fig. 2d) and TRP 21, LYS 78, ASN 161, and GLN 184. Also, this

compound showed Pi-Sigma, Pi-Pi Stacked, Pi-Pi T-shaped, and Pi-Alkyl interactions with important residues. In addition to this, a strong interaction of luteolin-7-rutinoside (Fig. 2c) with the target protein was observed, and also showed strong hydrogen bond interaction with HIS 111, VAL 48, TRP 21, ASN 161, SER 211, and ASP 217. Similarly, other interactions like Pi-Pi Stacked, Pi-Pi T-shaped, Pi-Alkyl, and Pi-Donor hydrogen bond interactions with amino acid residues were displayed. Engeletin (Fig. 2a), luteolin-7-O-glucoside (Fig. 2b), and scolymoside (Fig. 2e) showed a proper binding affinity with the enzyme's catalytic diads through hydrogen bond interactions and other crucial interactions. Isoangustone A, irigenin, desmanthin-I, and lucidin, exhibited significant interactions with both diads, forming hydrogen bonding interactions and various other bonds with amino acid residues (Fig. S3) & (Fig. S4) (vii, viii, ix, x, xi, xii). In comparison with other metabolites, myrciacitrin IV exhibited the least interaction distance (1.90 Å). After analysing the interaction with the diads on both proteins and the binding affinity top five listed metabolites were screened, and among them, myrciacitrin IV shows better results.

Toxicity Level Analyses

The web server Pro Tox II categorizes toxicity into six classes based on LD_{50} values, where classes I and II are considered fatal, class III is toxic, class IV is harmful, and classes V and VI are deemed not harmful (non-toxic) (Banerjee *et al.*, 2018). The top five metabolites which are notably, engeletin, luteolin-7-O-glucoside, luteolin-7-rutinoside, myrciacitrin IV, and scolymoside (Table 3) exhibited the least IC_{50} value, fall into either class V or VI emphasizing their potential lower toxicity. All the toxicity profiles of 90 metabolites were tabulated in Table S4.

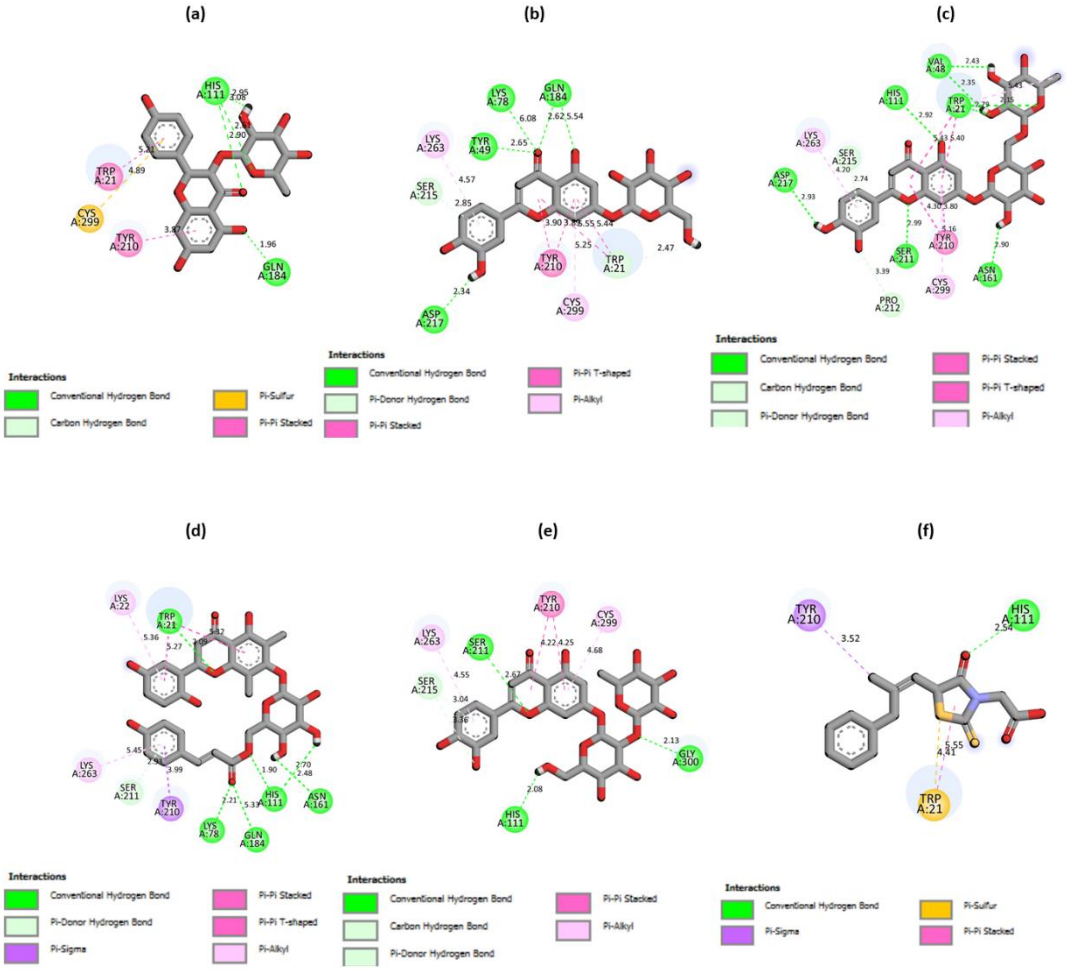

Figure 2. 2D interaction structures of (a) engeletin and (b) luteolin-7-o-glucoside (c) luteolin-7-rutinoside (d) myrciacitrin IV (e) Scolymoside (f) epalrestat complexed with 3O3R.

Table 2. Interaction of secondary metabolites with rat lens aldose reductase PDB ID: 3O3R

Metabolites	Binding Affinity (kcal/mol) 3o3R	Amino Acid Residues	Interaction Distance Å
epalrestat	-8.1	**TYR 48, HIS 110**, PHE 122, TRP 20, TYR 48	2.20, 2.13, 5.96, 7.01, 4.56
engeletin	-9.5	**HIS 111**, GLN 184, TRP 21, TYR 210, CYS 299	2.90, 2.61, 2.95, 3.08, 1,96, 5.21, 3.87, 4.89,
luteolin-7-O-glucoside	-10.4	**TYR 49**, LYS 78, GLN 184, ASP 217, TYR 210, SER 215 TRP 21, CYS 299, LYS 263	2.65, 6.08, 2.62, 5.54, 2.34, 3.90, 3.89, 2.85, 5.55, 5.44, 2.47, 5.25, 4.57
luteolin-7-rutinoside	-11.8	**HIS 111**, VAL 48, TRP 21, ASN 161, SER 211, ASP 217, SER 215, PRO 212, TYR 210, CYS 299, LYS 263	2.92, 2.43, 2.35, 2.79, 2.15, 5.43 5.40, 5.43, 2.90, 2.99, 2.93, 2.74, 3.39, 4.30, 3.80,4.20, 5.16
myrciacitrin IV	-11.8	**HIS 111**, ASN 161, GLN 184, LYS 78, TRP 21, TYR 210, SER 211, LYS 263, LYS 22	1.90, 2.48, 2.70, 5.33, 2.21, 2.09, 5.32, 5.27, 3.99, 2.93, 5.45, 5.36
scolymoside	-9.7	**HIS 111**, GLY 300, SER 211, TYR 210, SER 215, LYS 263, CYS 299	2.08, 2.13, 2.67, 4.22, 4.25, 3.04, 3.36,4.55, 4.68

Table 3. Toxicity table of secondary metabolites

Secondary Metabolites	Plants sources	IC_{50} value	LD_{50}(mg/kg)	Toxicity Class	Active Target	Probability
engeletin	*Stelechocarpus cauliflorus*	1.16	2300	5	Carcinogenicity Immunotoxicity Aryl hydrocarbon Receptor (AhR)	0.50 0.91 0.55
luteolin-7-O-glucoside	*Colocasia esculenta*	7.47	5000	5	Phosphoprotein (Tumor Supressor) p53	0.50
luteolin-7-rutinoside	*Colocasia esculenta*	2.59	5000	5	Immunotoxicity	0.93
myrciacitrin IV	*Myrcia multiflora*	0.79	2300	5	Immunotoxicity	0.99
scolymoside	*Artemisia montana*	0.55	5000	5	Immunotoxicity	0.98

Pharmacokinetics Properties Analyses

The most difficult issue in drug discovery research and development is going from lead to clinical therapeutic candidate. Medication needs to be very selective, have few side effects, and have enough biodistribution and bioavailability (Hefti, 2008) to enable the body to react as it needs to. Pharmacological potency, characteristics, and associated safety issues were evaluated (Table S3) by the pkCSM tool.

Drug bioavailability is affected by water solubility, and the optimal range is -5 to 0 (Putri *et al*., n.d.). Interestingly, the selected compounds (Table 4) exhibit good water solubility. The permeability of the colon cancer cell line (Caco-2) is examined to evaluate the absorption and bioavailability of oral drugs (Lagorce *et al*., 2017), and it shows that all metabolites have Caco-2 > -5.15 log unit, which represents appropriate permeability. The metabolites demonstrated varying levels of human intestinal absorption, exceeding 30%, except for luteolin-7-rutinoside and scolymoside. The drug is said to be well distributed in the plasma if a steady-state volume distribution (VDss) value > 0.5, while a lower value < -0.5 suggests a weak ability of drugs to cross the cell membrane (El-Shamy *et al*., 2022). VDss evaluation predicts except for epalrestat, all other metabolites are well distributed across the cell membrane. The selected metabolites do not cross the BBB because compounds with a logBB ≤ 0.3 are not sufficiently distributed to the brain (Muehlbacher *et al*., 2011). Only epalrestat, isoangustone A, lucidumol A, and tingenin B showed CNS permeability. Metabolism analysis revealed that only isoangustone A acted as a positive inhibitor for CYP1A2, CYP2C19, and CYP2C9 enzymes. Similarly, for excretion, tingenin B exhibited positive remarks for hepatotoxicity, while all metabolites showed negative results for AMES, Renal OCT substrate, and hepatotoxicity.

Table 4. ADMET profiles for secondary metabolites

	Secondary metabolites	epalrestat	engeletin	luteolin-7-rutinoside	luteolin-7-O-glucoside	myrciacitrin IV	scolymoside
Absorption	Water solubility (Log mol/L)	-3.144	-3.188	-2.904	-2.716	-2.972	-2.889
	Caco-2 Permeability (Log Papp 10^{-6} cm/s)	1.31	0.408	-1.523	0.248	-0.193	-1.188
	Intestinal absorption (% absorbed)	89.553	58.658	25.033	37.556	60.015	16.948
	Skin permeability (log Kp)	-2.735	-2.735	-2.735	-2.735	-2.735	-2.735
Distribution	VDss(Human, log L/kg)	-0.667	1.122	2.023	0.884	1.632	1.379
	BBB permeability (log BB)	0.108	-0.991	-1.979	-1.564	-2.013	-1.96
	CNS permeability (log PS)	-2.323	-4.014	-4.889	-3.93	-3.982	-4.96
Metabolism	CYP1A2	No	No	No	No	No	No
	CYP2C19	No	No	No	No	No	No
	CYP2C9	No	No	No	No	No	No
	CYP2D6	No	No	No	No	No	No
	CYP3A4	No	No	No	No	No	No
Excretion	Total clearance	0.11	0.046	-0.226	0.478	-0.227	-0.215
Toxicity	Ames Toxicity	No	No	No	No	No	No
	Hepatotoxicity	No	No	No	No	No	No
	Rat Oral Toxicity (LD_{50})	3.006	2.531	2.515	2.547	2.554	2.501

Density Functional Theory Calculations Analyses

The DFT technique involves performing semi-empirical molecular orbital calculations at the ground state to comprehend the energetic performance of chosen metabolites (Khatun *et al.*, 2024). The difference in energy between the highest occupied molecular orbital (HOMO) and the lowest unoccupied molecular orbital (LUMO) serves as an indicator, providing information about the compound's excitation energy and predicting electronic transition absorption in molecular structures (Hassan *et al.*, 2024). These molecular orbitals offer detailed insights into molecules' reactivity, and physical, and structural features (Samuel *et al.*, 2021). Myrciacitrin IV (3.379 eV) exhibited the least band gap energy compared to the standard epalrestat (3.191 eV) and the other metabolites (Table 5). In addition to band gap energy, other electronic calculations were also carried out, and the results suggest that myrciacitrin IV has better reactivity against the target protein.

Table 5. The variable quantum chemical parameters of the selected metabolites

Metabolites	Metabolites Optimized energy (Hartree)	E_{HOMO} (eV)	E_{LUMO} (eV)	Energy Gap ΔE (eV)	Electro-negativity χ (eV)	Pauling hardness η (e V)	Global softness ∑ (eV- 1)	Global electrophilicity ω (eV)	Dipole moment (Debye)
epalrestat	-1655.936	-6.110	-2.919	3.191	4.514	1.595	0.626	16.259	6.343
engeletin	-1565.214	-6.408	-2.109	4.299	4.258	2.149	0.465	19.493	2.727
luteolin-7-O-glucoside	-1639.198	-6.107	-2.075	4.031	4.090	2.015	0.496	16.868	11.056
luteolin-7-rutinoside	-2174.561	-5.949	-1.891	4.058	3.920	2.029	0.492	15.591	11.246
myrciaictrin IV	-2215.913	-5.502	-2.121	3.379	3.811	1.689	0.591	12.278	4.538
scolymoside	-2174.562	-6.218	-2.194	4.024	4.206	2.012	0.497	17.797	8.100

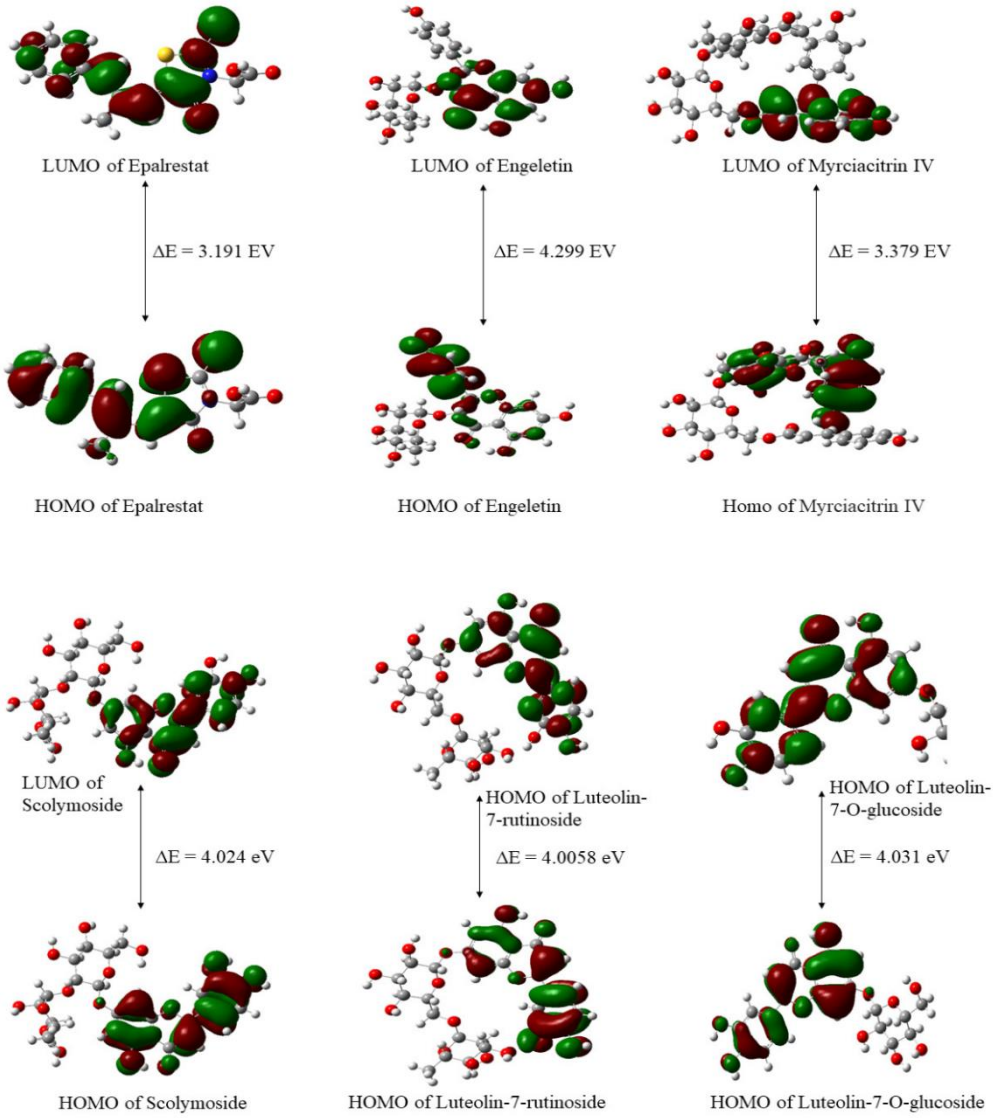

Figure 3. Comparison of band gap energy of the epalrestat, engeletin, myrciacitrin IV, luteolin-7-rutinoside, luteolin-7-O-glucoside, and scolymoside.

Molecular Dynamics Simulation Analyses

Root Mean Square Deviation (RMSD)

The RMSD of the six ligands with the target protein showed that the equilibrium reached 20 ns (Fig. 4A), but in the luteolin-7-O-rutinoside complex, equilibrium was achieved at 60 ns. The myrciacitrin IV complex had the most stable curve of all, with an RMSD of about 1.5 Å. This demonstrated that throughout the production run, the protein maintained its stable conformation and even bound with ligands. The RMSDs obtained for luteolin-7-rutinoside, luteolin-7-O-glucoside, engeletin, epalrestat, and scolymoside complex were found to be 1.5, 1.1, 2.3, 1.7, and 1.6 Å, respectively. Although the average RMSD of the luteolin-7-O-glucoside complex is slightly lower compared to the myrciacitrin complex, the myrciacitrin complex constant RMSD throughout the 100 ns simulation trajectory. While conducting the calculation of RMSD, sharp spikes were considered of concern (Karmakar *et al.*, 2024).

Radius of Gyration (R_g)

R_g measures the ligand-protein complex's compactness (Rampogu *et al.*, 2022), a smaller gyration radius suggests a more folded and compact structure while a high R_g value represents a more exposed and unfolded protein. The R_g calculation demonstrated that the complex system was shown to be sufficiently stable, with an observed value of 1.935 nm (Fig. 4B).

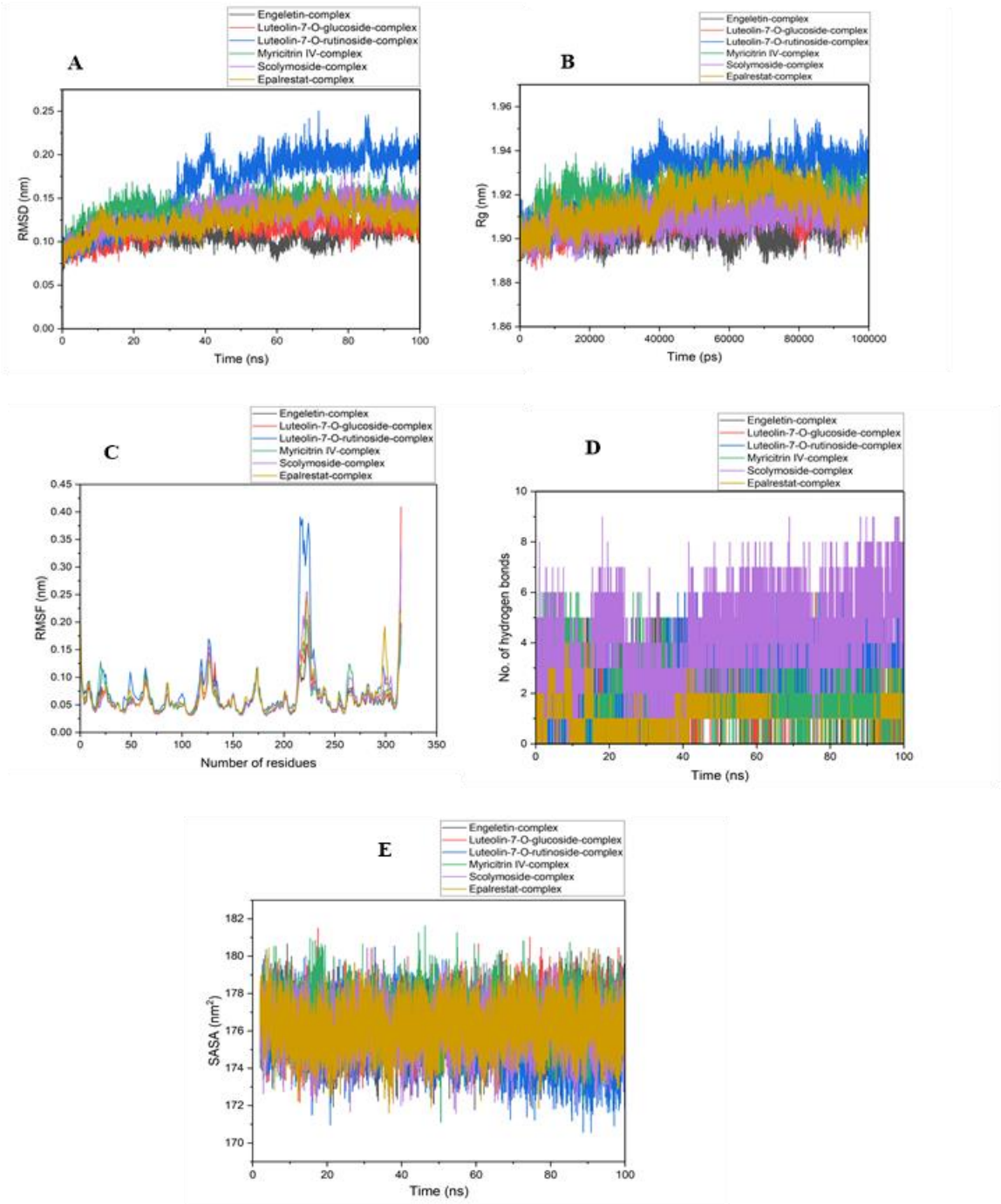

Figure 4. Different parameters obtained from 100 ns MD simulations trajectories of protein-ligand complexes (A) RMSD of protein-ligand complex, (B) Rg of protein, (C) RMSF of alpha carbon atoms, (D) Hydrogen bond count between ligand and key amino acid residues, and (E) SASA of protein (PDB ID 4JIR).

Root Mean Square Fluctuations (RMSF)

The flexibility of amino acid residues is determined by the RMSF. Since, RMSF enables the computation of the average change detected over a large number of atoms to estimate the displacement of a specific atom compared to the reference structure, it is essential for tracking local protein changes (Ahammad *et al.*, 2021). Higher RMSF values reflect regions of greater flexibility, such as loops and turns, while lower values indicate more rigid and stable secondary structures like α-helices and β-sheets (Sharma & Tamta, 2021). According to the RMSF values acquired for each residue around the ligand in the protein complex (Fig. 4C), the MD simulations demonstrated that the binding pocket was comparatively stable (Rampogu *et al.*, 2022). From the comparative plot generated, almost all residues of protein binding with myrciacitrin IV were less fluctuated, which suggests complex forms with a stable conformation throughout the simulation period. Amino acid residues of protein-ligand complex from 210 to 235 showed the highest fluctuations, suggesting the greater flexibility of protein, and these were not part of the catalytic diad. The results

of RMSF suggest that all the ligands bind strongly in the catalytic center of the protein.

Hydrogen bond count

The variations in the number of hydrogen bonds created between the ligand and the amino acid residue during the MD simulations are evaluated through a hydrogen bond plot. The number of hydrogen bonds in selected protein-ligand complexes ranges from 0 to 9 (Fig. 4D). The number of hydrogen bonds in the scolymoside complex peaked at nine at eighteen nanoseconds and stayed steady until the very end. The myricitrin IV-complex's hydrogen bond count was first measured at six and remained steady at three until 100 ns. The absence of hydrogen bonds at several locations after 60 ns, however, suggests that the adduct in the epalrestat complex is unstable.

Solvent Accessible Surface Area (SASA)

The SASA represents the area of protein available for interaction with the solvent and also the compactness of the protein-ligand complex. The proteins toward the end of MD simulations have an SASA of 171–182 nm^2 (Fig. 4E). Nearly every one of the six complexes looked like the constant value. There were minimal variations in the luteolin-7-O-rutinoside complex between 70 and 90 ns. According to the SASA, this result implies that the protein surface is more stable. However, the post simulation results showed that the chosen ligands do not expose the buried hydrophobic surface, suggesting good stability of the protein-ligand complex.

Binding Free Energy (BFE) Analysis:

A crucial component of hit-to-lead and lead optimization initiatives in the drug development process is optimizing binding affinity, selectivity, and other off-target interactions. By calculating free energy differences among similar molecules, relative binding free energy (RBFE) computations provide an appealing method of predicting protein-ligand binding affinities *in silico* using statistical mechanics and molecular simulations (Cournia, Allen, & Sherman, 2017). The prime MM/GBSA approach was used to measure the binding free energy of the six ligands with the protein (PDB ID 4JIR), which computes the absolute BFE to estimate the strength of the protein-ligand interaction (Genheden & Ryde, 2015). The scolymoside complex exhibits lower binding energy, followed by luteolin7-rutinoside, myrciacitrin IV, and so on, with binding energies ΔG_{bind} = -34.11, -32.75, -28.13 kcal/mol, respectively (Table 6), indicating strong interaction with the target protein, which supported the molecular docking and conformational dynamics investigations.

Table 6. Binding free energy of six ligands with protein (PDB ID 4JIR).

Secondary Metabolites	Binding free energy (ΔG_{bind}) ($Kcalmol^{-1}$)
engeletin	-23.08
luteolin-7-O-glucoside	-26.29
luteolin-7-rutinoside	-32.75
myrciacitrin IV	-28.13
scolymoside	-34.11

CONCLUSIONS

Natural aldose reductase inhibitors were gathered based on recorded IC_{50} values of secondary metabolites from plants. Five metabolites with binding energies below -9.0 kcal/mol, proper interaction with both proteins, and toxicity class V were short-listed as potential drug candidates. All displayed negative inhibition to the cytochrome family, favourable absorption, permeability, and negative results for AMES and hepatotoxicity. Analysing their IC_{50} values, all five exhibited values below 10 μM. Among them is myrciacitrin IV, with outstanding interaction and the least band gap energy (3.379 eV). The MD simulations provided useful information about the radius of gyration, SASA, RMSD, RMSF, hydrogen bond count, and binding free energy of the protein-ligand complex, which favoured myrciacitrin IV, making it a promising candidate for diabetes drug development. Although this finding suggests a promising aldose reductase inhibitor, further research is necessary for innovative diabetes control treatments in conjunction with other therapeutic approaches.

ACKNOWLEDGEMENTS

Ranju Khatiwada thanks the University Grants Commission, Nepal, for funding (UGC Master's Research Support award no: MRS-78-79-S&T-24).

AUTHORS' CONTRIBUTION

Ranju Khatiwada and Rezina Pradhan investigated the study; Asmita Shrestha proposed the methodology; Ranju Khatiwada, Asmita Shrestha, Siddha Raj Upadhyaya, Ashish Phuyal, and Sishir Bikram KC performed a formal analysis; Kabita Gyawali and Siddha Raj Upadhyaya were responsible for the resources; Ranju Khatiwada, Asmita Shrestha, and Ashish Phuyal wrote the original draft; Khaga Raj Sharma and Niranjan Parajuli supervised the project and revised the manuscript.

CONFLICT OF INTEREST

The authors declare that they have no conflicts of interest.

DATA AVAILABILITY

The data that support the findings of this study are available from the corresponding author upon reasonable request.

SUPPLEMENTARY MATERIALS

(Table S1) Interaction of secondary metabolites with protein 4JIR; (Table S2) Interaction of secondary metabolites with 3O3R; (Table S3) ADMET analysis of secondary metabolites; (Table S4) Toxicity profile of Secondary Metabolites; (Fig. S1) 2D interaction of (i) Epalrestat (ii) Engeletin (iii) Luteolin-7-O-glucoside (iv) Luteolin-7-rutinoside (v) Myrciacitrin IV (vi) Scolymoside (vii) Tingenin B with 4JIR; (Fig. S2) 3D interaction of (i) Epalrestat (ii) Engeletin (iii) Luteolin-7-O-glucoside (iv) Luteolin-7-rutinoside (v) Myrciacitrin IV (vi) Scolymoside (vii) Tingenin B with 4JIR; (Fig. S3) 2D interaction of (i) Epalrestat (ii) Engeletin (iii) Luteolin-7-O-glucoside (iv) Luteolin7-rutinoside (v)

Scolymoside (vi) Tingenin B with 3O3R; (Fig. S4) 3D interaction of (i) Epalrestat (ii) Engeletin (iii) Luteolin-7-O-glucoside (iv) Luteolin7-rutinoside (v) Scolymoside (vi) Tingenin B with 3O3R.

REFERENCES

Abraham, M.J., Murtola, T., Schulz, R., Páll, S., Smith, J.C., Hess, B., & Lindahl, E. (2015). GROMACS: High performance molecular simulations through multi-level parallelism from laptops to supercomputers. *SoftwareX*, *1–2*, 19–25. https://doi.org/10.1016/j.softx.2015.06.001

Abu-Melha, S. (2018). Design, synthesis and DFT/DNP modeling study of New 2-Amino-5-arylazothiazole derivatives as potential antibacterial agents. *Molecules*, *23*(2), 434. https://doi.org/10.3390/molecules23020434

Agu, P.C., Afiukwa, C.A., Orji, O.U., Ezeh, E.M., Ofoke, I.H., Ogbu, C.O., … & Aja, P.M. (2023). Molecular docking as a tool for the discovery of molecular targets of nutraceuticals in diseases management. *Scientific Reports*, *13*(1), 13398. https://doi.org/10.1038/s41598-023-40160-2

Ahammad, F., Alam, R., Mahmud, R., Akhter, S., Talukder, E.K., Tonmoy, A.M., … & Qadri, I. (2021). Pharmacoinformatics and molecular dynamics simulation-based phytochemical screening of neem plant *(Azadiractha indica)* against human cancer by targeting MCM7 protein. *Briefings in Bioinformatics*, *22*(5), bbab098. https://doi.org/10.1093/bib/bbab098

Antonetti, D.A., Klein, R., & Gardner, T.W. (2012). Diabetic retinopathy. *New England Journal of Medicine*, *366*(13), 1227–1239. https://doi.org/10.1056/NEJMra1005073

Banditelli, S., Boldrini, E., Vilardo, P.G., Cecconi, I., Cappiello, M., Dal monte, M., … & Mura, U. (1999). A New approach against sugar cataract through aldose reductase inhibitors. *Experimental Eye Research*, *69*(5), 533–538. https://doi.org/10.1006/exer.1999.0729

Banerjee, P., Eckert, A.O., Schrey, A.K., & Preissner, R. (2018). ProTox-II: A webserver for the prediction of toxicity of chemicals. *Nucleic Acids Research*, *46*(W1), W257–W263. https://doi.org/10.1093/nar/gky318

Brownlee, M. (2005). The pathobiology of diabetic complications. *Diabetes*, *54*(6), 1615–1625. https://doi.org/10.2337/diabetes.54.6.1615

Bugnon, M., Goullieux, M., Röhrig, U.F., Perez, M.A.S., Daina, A., Michielin, O., & Zoete, V. (2023). SwissParam 2023: A modern web-based tool for efficient small molecule parametrization. *Journal of Chemical Information and Modeling*, *63*(21), 6469–6475. https://doi.org/10.1021/acs.jcim.3c01053

Ciulla, T.A., Amador, A.G., & Zinman, B. (2003). Diabetic retinopathy and diabetic macular edema: pathophysiology, screening, and novel therapies. *Diabetes Care*, *26*(9), 2653–2664. https://doi.org/10.2337/diacare.26.9.2653

Cournia, Z., Allen, B., & Sherman, W. (2017). Relative binding free energy calculations in drug discovery: Recent advances and practical considerations. *Journal of Chemical Information and Modeling*, *57*(12), 2911–2937. https://doi.org/10.1021/acs.jcim.7b00564

Dwivedi, A., Baboo, V., & Bajpai, A. (2015). Fukui function analysis and optical, electronic, and vibrational properties of tetrahydrofuran and its derivatives: A complete quantum chemical study. *Journal of Theoretical Chemistry*, *2015*, e345234. https://doi.org/10.1155/2015/345234

Ekins, S., Mestres, J., & Testa, B. (2007). In silico pharmacology for drug discovery: Methods for virtual ligand screening and profiling. *British Journal of Pharmacology*, *152*(1), 9–20. https://doi.org/10.1038/sj.bjp.0707305

El-Shamy, N.T., Alkaoud, A.M., Hussein, R.K., Ibrahim, M.A., Alhamzani, A.G., & Abou-Krisha, M.M. (2022). DFT, ADMET and molecular docking investigations for the antimicrobial activity of 6,6'-Diamino-1,1',3,3'-tetramethyl-5,5'-(4-chlorobenzylidene)bis[pyrimidine-2,4(1H,3H)-dione]. *Molecules*, *27*(3), 620. https://doi.org/10.3390/molecules27030620

Ferreira, L.G., Dos Santos, R.N., Oliva, G., & Andricopulo, A.D. (2015). Molecular docking and structure-based drug design strategies. *Molecules (Basel, Switzerland)*, *20*(7), 13384–13421. https://doi.org/10.3390/molecules200713384

Ganesan, A., Coote, M.L., & Barakat, K. (2017). Molecular dynamics-driven drug discovery: Leaping forward with confidence. *Drug Discovery Today*, *22*(2), 249–269. https://doi.org/10.1016/j.drudis.2016.11.001

Garg, A., Tadesse, A., & Eswaramoorthy, R. (2021). A four-component domino reaction: An eco-compatible and highly efficient construction of 1,8-naphthyridine derivatives, their *In Silico* molecular docking, drug likeness, ADME, and toxicity studies. *Journal of Chemistry*, *2021*, e5589837. https://doi.org/10.1155/2021/5589837

Genheden, S., & Ryde, U. (2015). The MM/PBSA and MM/GBSA methods to estimate ligand-binding affinities. *Expert Opinion on Drug Discovery*, *10*(5), 449–461. https://doi.org/10.1517/17460441.2015.1032936

Geraldes, P., & King, G.L. (2010). Activation of protein kinase C isoforms and its impact on diabetic complications. *Circulation Research*, *106*(8), 1319–1331. https://doi.org/10.1161/CIRCRESAHA.110.217117

Giacco, F., & Brownlee, M. (2010). Oxidative stress and diabetic complications. *Circulation Research*, *107*(9), 1058–1070. https://doi.org/10.1161/CIRCRESAHA.110.223545

Grewal, A.S., Bhardwaj, S., Pandita, D., Lather, V., & Sekhon, B.S. (2016). Updates on aldose reductase inhibitors for management of diabetic complications and non-diabetic diseases. *Mini Reviews in Medicinal Chemistry*, *16*(2), 120–162. https://doi.org/10.2174/1389557515666150909143737

Grewal, A.S., Thapa, K., Kanojia, N., Sharma, N., & Singh, S. (2020). Natural compounds as source of aldose reductase (ar) inhibitors for the treatment of

diabetic complications: A mini review. *Current Drug Metabolism*, *21*(14), 1091–1116. https://doi.org/10.2174/1389200221666201016124125

Hassan, A.U., Sumrra, S.H., Mustafa, G., Mohyuddin, A., Imran, M., Mehmood, R.F., & Mohyuddin, A. (2024). Novel pull–push solar switches with a D-π-D-π-A framework of the thiophene core: Computed absorbance/fluorescence ability with device parameters. *Structural Chemistry*, *35*(1), 47–64. https://doi.org/10.1007/s11224-023-02172-6

Hefti, F.F. (2008). Requirements for a lead compound to become a clinical candidate. *BMC Neuroscience*, *9*(3), S7. https://doi.org/10.1186/1471-2202-9-S3-S7

Hendrick, A.M., Gibson, M.V., & Kulshreshtha, A. (2015). Diabetic retinopathy. *Primary Care: Clinics in Office Practice*, *42*(3), 451–464. https://doi.org/10.1016/j.pop.2015.05.005

Karmakar, R., Chatterjee, S., Datta, D., & Chakraborty, D. (2024). Application of harmony search algorithm in optimizing autoregressive integrated moving average: A study on a data set of Coronavirus Disease 2019. *Systems and Soft Computing*, *6*, 200067. https://doi.org/10.1016/j.sasc.2023.200067

Khatun, S., Bhagat, R.P., Amin, S.A., Jha, T., & Gayen, S. (2024). Density functional theory (DFT) studies in HDAC-based chemotherapeutics: Current findings, case studies and future perspectives. *Computers in Biology and Medicine*, *175*, 108468. https://doi.org/10.1016/j.compbiomed.2024.108468

Kitchen, D.B., Decornez, H., Furr, J.R., & Bajorath, J. (2004). Docking and scoring in virtual screening for drug discovery: Methods and applications. *Nature Reviews. Drug Discovery*, *3*(11), 935–949. https://doi.org/10.1038/nrd1549

Klein, R., Klein, B.E.K., & Moss, S.E. (1989). The wisconsin epidemiological study of diabetic retinopathy: A review. *Diabetes/Metabolism Reviews*, *5*(7), 559–570. https://doi.org/10.1002/dmr.5610050703

Kolb, P., Ferreira, R.S., Irwin, J.J., & Shoichet, B.K. (2009). Docking and chemoinformatic screens for new ligands and targets. *Current Opinion in Biotechnology*, *20*(4), 429–436. https://doi.org/10.1016/j.copbio.2009.08.003

Lagorce, D., Douguet, D., Miteva, M.A., & Villoutreix, B.O. (2017). Computational analysis of calculated physicochemical and ADMET properties of protein-protein interaction inhibitors. *Scientific Reports*, *7*(1), 46277. https://doi.org/10.1038/srep46277

Macalino, S.J.Y., Gosu, V., Hong, S., & Choi, S. (2015). Role of computer-aided drug design in modern drug discovery. *Archives of Pharmacal Research*, *38*(9), 1686–1701. https://doi.org/10.1007/s12272-015-0640-5

Maccari, R., & Ottanà, R. (2015). Targeting Aldose Reductase for the Treatment of Diabetes Complications and Inflammatory Diseases: New Insights and Future Directions. *Journal of Medicinal Chemistry*, *58*(5), 2047–2067. https://doi.org/10.1021/jm500907a

Mori, S., Kubo, S., Akiyoshi, T., Yamada, S., Miyazaki, T., Hotta, H., … & Shigemoto, K. (2012). Antibodies against muscle-specific kinase impair both presynaptic and postsynaptic functions in a murine model of myasthenia gravis. *The American Journal of Pathology*, *180*(2), 798–810. https://doi.org/10.1016/j.ajpath.2011.10.031

Muehlbacher, M., Spitzer, G.M., Liedl, K.R., & Kornhuber, J. (2011). Qualitative prediction of blood-brain barrier permeability on a large and refined dataset. *Journal of Computer-Aided Molecular Design*, *25*(12), 1095–1106. https://doi.org/10.1007/s10822-011-9478-1

Nagini, S., Kallamadi, P.R., Tanagala, K.K.K., & Reddy, G.B. (2024). Aldo-keto reductases: Role in cancer development and theranostics. *Oncology Research*, *32*(8), 1287–1308. https://doi.org/10.32604/or.2024.049918

Putri, S.A., Julaeha, E., Kagawa, N., & Kurnia, D. (n.d.). *Phenolic Compounds from Ocimum basilicum Revealed as Antibacterial by Experimental and Computational Screening-Based Studies against Oral Infections*. https://doi.org/10.1155/2024/3696250

Rampogu, S., Lee, G., Park, J.S., Lee, K.W., & Kim, M.O. (2022). Molecular docking and molecular dynamics simulations discover curcumin analogue as a plausible dual inhibitor for SARS-CoV-2. *International Journal of Molecular Sciences*, *23*(3), 1771. https://doi.org/10.3390/ijms23031771

Samuel, Y., Garg, A., & Mulugeta, E. (2021). Synthesis, DFT analysis, and evaluation of antibacterial and antioxidant activities of sulfathiazole derivatives combined with in silico molecular docking and ADMET predictions. *Biochemistry Research International*, *2021*(1), 7534561. https://doi.org/10.1155/2021/7534561

Sarges, R., Schnur, R.C., Belletire, J.L., & Peterson, M.J. (1988). Spiro hydantoin aldose reductase inhibitors. *Journal of Medicinal Chemistry*, *31*(1), 230–243. https://doi.org/10.1021/jm00396a037

Sastry, G.M., Adzhigirey, M., Day, T., Annabhimoju, R., & Sherman, W. (2013). Protein and ligand preparation: Parameters, protocols, and influence on virtual screening enrichments. *Journal of Computer-Aided Molecular Design*, *27*(3), 221–234. https://doi.org/10.1007/s10822-013-9644-8

Sestanj, K., Bellini, F., Fung, S., Abraham, N., Treasurywala, A., Humber, L., … & Dvornik, D. (1984). N-[[5-(Trifluoromethyl)-6-methoxy-1-naphthalenyl]thioxomethyl]-N-methylglycine (Tolrestat), a potent, orally active aldose reductase inhibitor. *Journal of Medicinal Chemistry*, *27*(3), 255–256. https://doi.org/10.1021/jm00369a003

Sharma, P., Tushar, J., Tanuja, J., Subhash, C., & Tamta, S. (2021). Molecular dynamics simulation for screening phytochemicals as α-amylase inhibitors from medicinal plants. *Journal of Biomolecular Structure and Dynamics*, *39*(17), 6524–6538. https://doi.org/10.1080/07391102.2020.1801507

Singh Grewal, A., Bhardwaj, S., Pandita, D., Lather, V., & Singh Sekhon, B. (2015). Updates on aldose reductase inhibitors for management of diabetic complications and non-diabetic diseases. *Mini-Reviews in Medicinal Chemistry*, *16*(2), 120–162. https://doi.org

/10.2174/1389557515666150909143737

Sundaram, K., Dhagat, U., Endo, S., Chung, R., Matsunaga, T., Hara, A., & El-Kabbani, O. (2011). Structure of rat aldose reductase-like protein AKR1B14 holoenzyme: Probing the role of His269 in coenzyme binding by site-directed mutagenesis. *Bioorganic & Medicinal Chemistry Letters*, *21*(2), 801–804. https://doi.org/10.1016/j.bmcl.2010.11.086

Valdés-Tresanco, M.S., Valdés-Tresanco, M.E., Valiente, P.A., & Moreno, E. (2021). gmx_MMPBSA: A new tool to perform end-state free energy calculations with GROMACS. *Journal of Chemical Theory and Computation*, *17*(10), 6281–6291. https://doi.org/10.1021/acs.jctc.1c00645

Wacha, A.F., & Lemkul, J.A. (2023). charmm2gmx: An automated method to port the CHARMM additive force field to GROMACS. *Journal of Chemical Information and Modeling*, *63*(14), 4246–4252. https://doi.org/10.1021/acs.jcim.3c00860

Zhang, L., Zhang, H., Zhao, Y., Li, Z., Chen, S., Zhai, J., … & Hu, X. (2013). Inhibitor selectivity between aldo–keto reductase superfamily members AKR1B10 and AKR1B1: Role of Trp112 (Trp111). *FEBS Letters*, *587*(22), 3681–3686. https://doi.org/10.1016/j.febslet.2013.09.031

Internet Source:

RCSB. (2025). RCSB Protein Data Bank**.** Retrieved February 25, 2025 from https://www.rcsb.org/.